best

Sustainable Bioenergy
Solutions for Tomorrow

RESEARCH REPORT
D1.4-5
HELSINKI 2015

Cyril Bajamundi[1], Timo Leino[1], Martti Aho[1],
Jouni Hämälainen[1], Merja Hedman[2], Juha Roppo[3]
[1] VTT Technical Research Centre of Finland
[2] Valmet Technologies Oy, [3] Enopsis Oy

Combustibility of Empty Fruit Bunch (EFB) Pellets in Circulating Fluidized Bed Combustion

Solution Architect for Global
Bioeconomy & Cleantech Opportunities

CLIC INNOVATION OY
ETELÄRANTA 10
P.O. BOX 10
FI-00131 HELSINKI,
FINLAND
CLICINNOVATION.FI

ISBN 978-952-5947-94-6

CLIC Innovation
Research report D1.4-5

Cyril Bajamundi [1], Timo Leino [1], Martti Aho [1], Jouni Hämälainen[1], Merja Hedman[2], Juha Roppo[3]
[1] VTT Technical Research Centre of Finland
[2] Valmet Technologies Oy, [3] Enopsis Oy

Combustibility of Empty Fruit Bunch (EFB) Pellets in Circulating Fluidized Bed Combustion

Sustainable Bioenergy Solutions for Tomorrow

Combustibility of EFB Pellets in CFB Combustion

Bajamundi C., Leino T., Aho M., Hämälainen J., Hedman M., Ruppo, J.

Name of the report: Combustibility of EFBs in Circulating Fluidized Bed Combustion

Key words: Empty Fruit Bunch Pellet, Combustion, Circulating Fluidized Bed, Corrosion, Emissions

Summary

Empty fruit bunch (EFB) pellet originating from the ASEAN was co-combusted with coal. The goal is to maximize the share of the EFB and assess emission, fouling and corrosion risks.

On emission, at low EFB share, limestone addition might be needed to keep the SO_2 concentration in the flue gas below the desired level; at higher shares, limestone may not be required. HCl concentration in the flue gas rose as more EFB is burned. N_2O concentration, which is typically elevated in coal combustion, drastically reduced with EFB en-%, which favored formation of NO.

One can assume that deposits are corrosive only if they contain Cl. The critical limit is approximately 35% EFB in energy. Probes simulating superheaters of power plants show continuous increase of deposition rate and potassium concentration with EFB energy portion. Other elements dominant in the deposits are Si, Al, and S. According to thermodynamic calculations, deposition rate, K and Cl increase is enhanced by formation of KCl in the flue gas coupled with deposit melting. The risk for corrosion begins at around 25 en-% to 35 en-% share of EFB depending on the material temperature and grade.

Helsinki, March 2016

CONTENTS

1 Introduction

By 2020, the European Union is expected to have the share of renewable resources in the final energy consumption at 20% [1]. Bioenergy is an integral renewable resource component required to meet this goal. In 2013, biomass is projected to account for more than half of renewable energy output in 2020. From 2002 to 2012, Eurostat [2] reports a continuous rise in primary energy production of biomass based energy, see Figure 1.

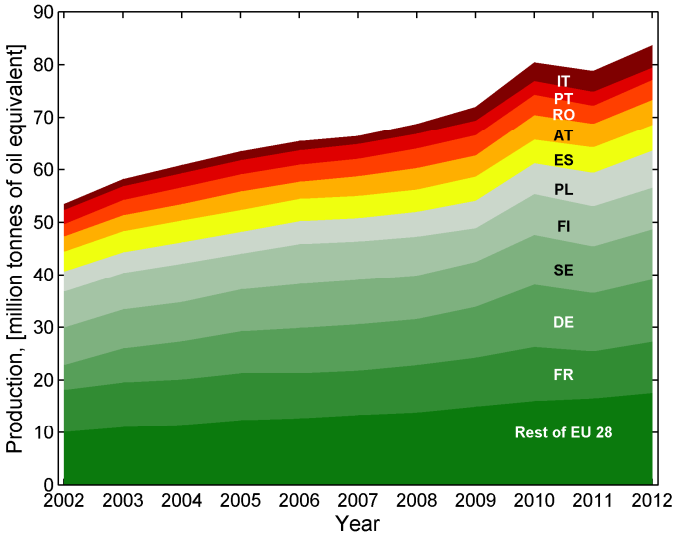

Figure 1: Primary production of biomass energy. Data from [2].

By 2020, the primary solid biomass use is expected to reach 146 – 158 Mtoe while the production is only 120 Mtoe. This equates to a supply gap of 25 – 40 Mtoe. To meet the targets, massive expansion of biomass power and heat generation will be required – both new build and the adaption or conversion of existing fossil plant [3].

Figure 2 gives an example of routes to convert biomass to energy. However, it does not describe well the situation in Scandinavia where large quantities of biomass is combusted in large power plants.

Combustion of biomass presents several operational challenges. For example, combustion of straw produces high KCl concentration that results to superheater corrosion[4–6]. Co-firing of 30 wt.-% grain waste, an agro-fuel, with wood fuel in a full-scale bubbling fluidized bed reactor led to heavy furnace-wall slagging due to increased potassium and phosphorous [7]. The key elements contributing to corrosion and ash melting are shown in Figure 3.

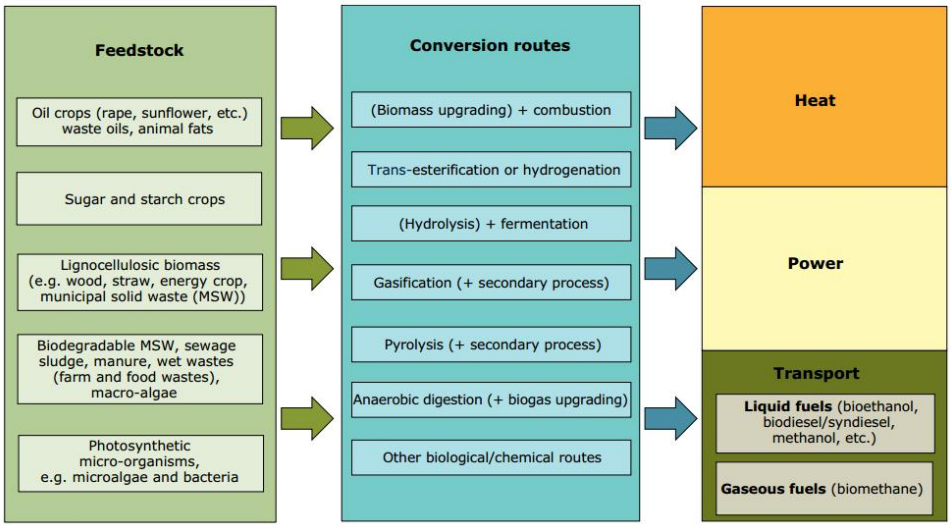

Figure 2: Routes for converting biomass to energy [1].

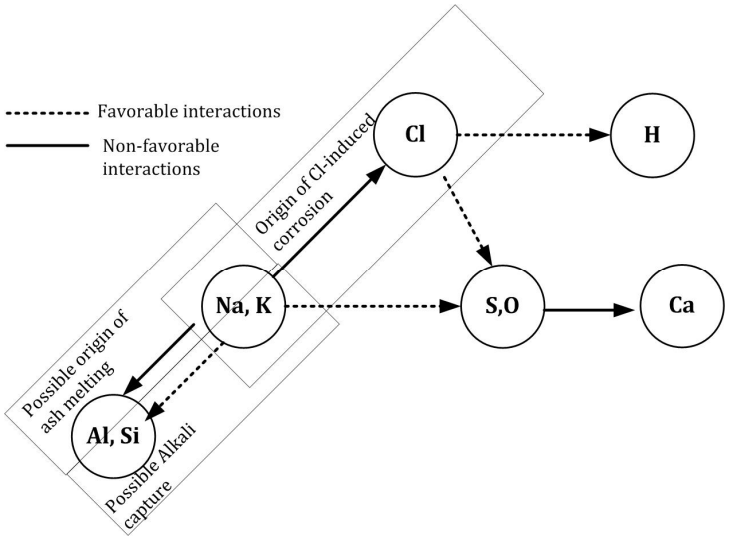

Figure 3. Key elements responsible for operational challenges during combustion of biomass.

Alkalis from the fuel react to form submicron aerosol particles that may condense at superheater conditions and attack the metal.

$$K_{fuel}, Na_{fuel} + Cl_{fuel} \rightarrow (K, Na)Cl_{(g)} \quad (1)$$

Meanwhile un-vaporized K and Na may combine with Al, Si in the fuel and form low melting point eutectic mixtures, see Table 1.

Table 1. Eutectic composition and temperature of binary salts and oxide systems estimated using FactSage 6.4 [8].

System and Composition, [mol/mol]	Eutectic Temperature, [°C]
0.957 SiO_2 – 0.043 Al_2O_3	1594
0.613 SiO_2 – 0.387 CaO	1437
0.050 Al_2O_3 – 0.950 Na_2O	1132
0.741 SiO_2 – 0.259 Na_2O	793
0.260 K_2SO_4 – 0.74 KCl	690
0.506 KCl – 0.494 NaCl	657
0.376 K_2CO_3 – 0.624 KCl	631

To combat these operation issues, additives can be added to prevent/destroy formation of problematic compounds. Reactive aluminosilicates and aluminosilicate-containing fuels (such as coal) and additives such as kaolinite and bauxite can also trap the alkalis via a chemisorption reaction[9]

$$2MCl + H_2O + Al_2O_3 \cdot xSiO_2 \rightarrow M_2O \cdot Al_2O_3 \cdot xSiO_2 + 2HCl \quad (2)$$

where $M = Na, K$

Peat ash addition has also been shown to significantly affect the chlorine content in the aerosols due to the interaction of K with the peat ash resulting in the reduced volatilization of the alkali [10] . Co-firing of peat can also lower the amount of alkali chlorides if the aluminosilicates present is “reactive”. Sludge is also a possible alkali-capture agent [5].

Addition of sulfur containing additives or fuels increases the formation of SO_2 or SO_3 in the furnace. Sulfur (as SO_2) attacks the alkali chlorides via the reaction [11]:

$$2MCl_{(s)} + SO_{2(g)} + \frac{1}{2}O_2 + H_2O_{(g)} \rightarrow M_2SO_{4(s)} + 2HCl_{(g)} \quad (3)$$

where $M = Na, K$

Meanwhile the presence of Ca in the combustion system may reduce the efficiency of alkali chloride sulfation and favor the production of $CaSO_{4(s)}$ [12]

$$CaO_{(s)} + SO_{2(g)} + \frac{1}{2}O_{2(g)} \rightarrow CaSO_{4(s)} \quad (4)$$

2 Objective

The main objective of this study is to develop competence in understanding emission formation, ash chemistry issues related to fouling and corrosion of agro-based fuels. Principal target is to maximise the share of agro fuels in power production. The fuel originates from ASEAN (Association of South East Asian Nations). Research methods includes pilot scale test run combined with emission and ash chemistry monitoring as well as chemical modelling.

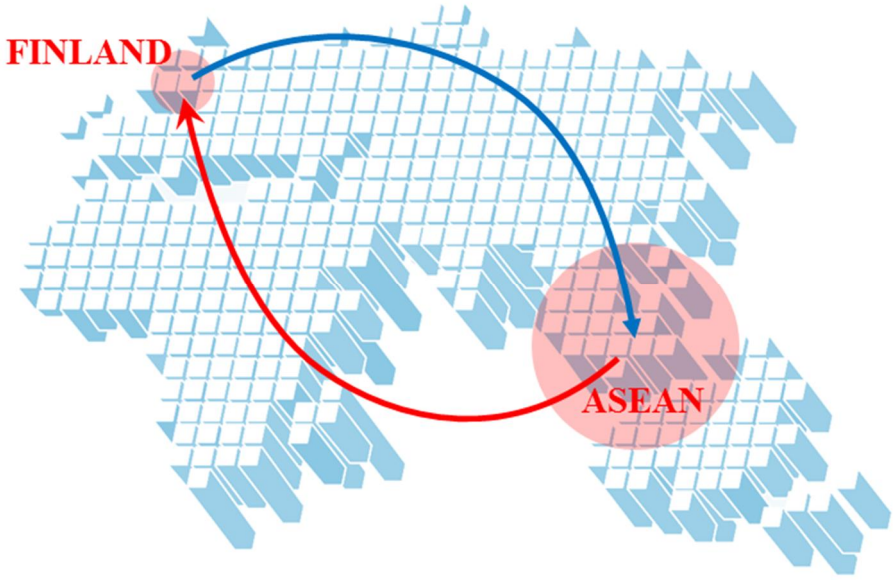

Figure 4: Geographical location of the origin of the agro-based fuel (ASEAN) and Finland.

3 Experimental

3.1 CFB-pilot experiments

The VTT's circulating fluidized bed combustor (CFB) pilot plant used in the Best-project is shown in Figure 5. In spite of the small size, this unique reactor creates temperature vs. residence time profiles similar to full scale CFB and air staging can be carried out as in power plants. In addition, mineral circulation is similar to power plants. The pilot can be operated in air combustion with fuel thermal input ranging typically between 40-60 kW. The height of the riser is 8 m and the inner diameter 170 mm. The combustor is equipped with several separately controlled electrically heated and water/air-cooled zones in order to control the process conditions (for example oxygen level, temperature and load) almost independently. Several ports for gas and solid material sampling are located in the freeboard area. Bed material (bottom ash) can be sampled via sampling tube and circulation material samples can be taken below the

primary cyclone or from the loop seal. Fly ash samples can be taken from the secondary cyclone, gas coolers and bag house filter. The combustor is controlled with an automation system on which all measurement data is stored.

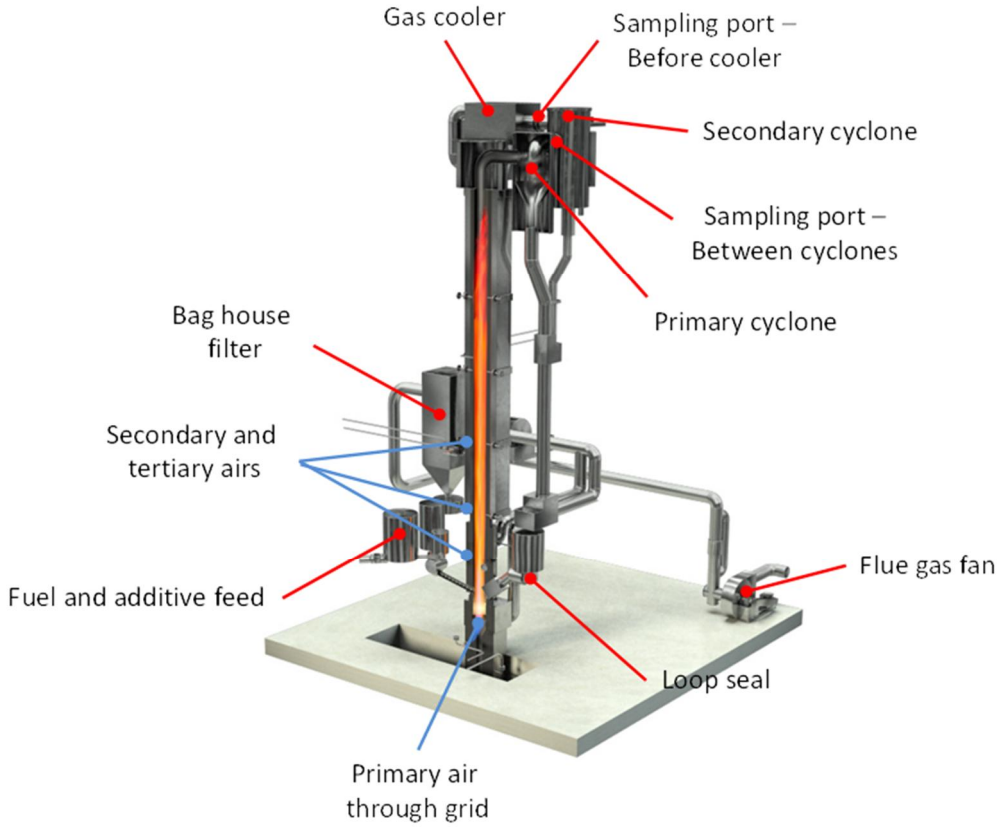

Figure 5: Schematic diagram of the pilot scale circulating fluidized bed combustor.

Fuel can be fed into the combustor through two separate fuel-feeding lines. There is also an own feeder for additives such as limestone. Fuel containers are mounted on the top of scales, which enables the determination of mass flow rates for solid fuels as a weight loss against time. The combustion air can be divided into primary, secondary and tertiary air. Oxygen concentration of the primary and secondary airs can be controlled by mixing nitrogen gas or recycled flue gas into the gas flows. The secondary and tertiary airs can be fed into three different levels of the combustor. The lowest feeding point (1.3 m above the air grid) for the secondary air is mainly used in the test runs and tertiary airs (at two levels) are mainly used in air staging tests.

The main flue gas compound measurements are measured with both FTIR-spectrometer and traditional on-line analyzers. Gas samples can also be taken with the FTIR-spectrometer from different levels of the freeboard and also before and after the cyclones, gas cooler and bag house filter. The traditional

on-line analyzers are connected to the flue gas duct between the gas cooler and bag house filter.

3.2 Fuels

The fuels selected for pilot scale CFB tests were Russian bituminous coal (provided by Valmet) and Empty Fruit Bunch (EFB) pellet from Asia. The ultimate and proximate fuel analyses are shown in Table 2.The EFB composition measured in this study is similar to the composition of the EFB reported by Lahijani et al.[13].

Cl concentration in the coal was very low. Coal can sometimes contain up to 0.1 wt % Cl. Low sulfur content in the Russian coal may lead to low capability to destroy corrosive alkali chlorides in the furnace. Free aluminum silicates in coal ash may destroy effectively corrosive alkali chlorides resulting in a good protecting power even without additional contribution from fuel-S.

Table 2: Ultimate and proximate analyses for the selected project fuels.

Analysis	unit	Russian coal	EFB pellet
Moisture content	wt%	6.6	7.5
HHV	MJ/kg, d.s.	28.4	20.4
LHV	MJ/kg, d.s.	27.4	19.1
Ash 815 C	wt% d.s.	16.2	8.0
Ash 550 C	wt% d.s.	16.8	9.1
Volatiles	wt% d.s.	32.8	72.3
C	wt% d.s.	68.3	48.5
H	wt% d.s.	4.6	5.8
N	wt% d.s.	2.22	1.14
S	wt% d.s.	0.36	0.12
Cl	wt% d.s.	0.005	0.53

The major elements (in oxide form) are shown in Figure 6. K_2O in EFB is very high compared to coal, while Al_2O_3 and SiO_2 are significantly high in the coal.

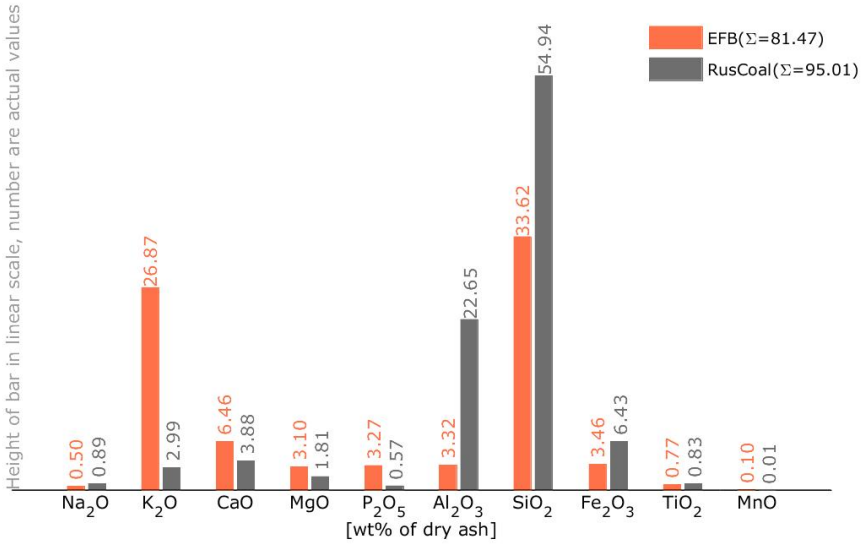

Figure 6. Concentration of major elements in the fuels studied. The sum of the concentration is given as Σ.

Chemical fractionation of the two fuels reveals the reactivity of the major elements of the fuels, see Figure 7. Water and acetic acid soluble fractions are considered reactive.

For the EFB (Figure 7 a), majority of K, Mg, and P (≥ 80%) are in the reactive fraction. Na and Ca in the reactive fraction is low (<40%). Al, Si, Fe, Ti are mostly present in the HCl and rest fraction – considered to be non-reactive.

For the coal (Figure 7 b), approximately 50% of Na are in the reactive fraction. K, P, Al, Si, Fe, Ti are mostly present in the HCl and rest fraction. The reactive fraction of Ca is high (~80%).

These analyses clearly show the difference between fuels. K and Cl, which form KCl, may come mostly from the EFB. As the energy share of EFB is increased corrosivity of the flue gas increases. The excessive reactive K in the EFB may also result in ash melting.

An additional interesting result was different forms of alkalis in EFB relative to coal. One can assume (without chemical fractionation results from S and Cl) that sodium is mostly bound in silicates in EFB whereas most of potassium is in silicates in the coal sample. One can also assume that KCl is an important compound of potassium in EFB (molar K/Cl ~ 3.4 and molar $K_{soluble}$/ Cl ~ 2.75).

Figure 8 shows the comparison of composition of major elements in the EFB and other biomass fuels. EFB is near the fuels with high melting propensity.

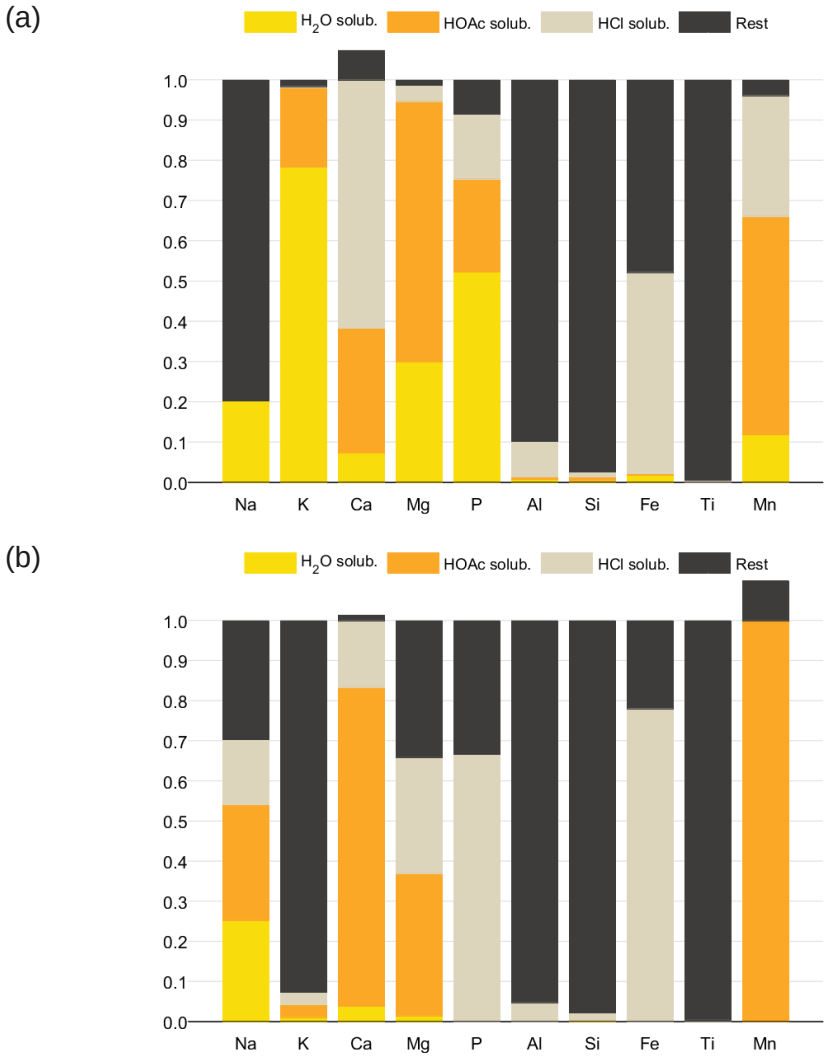

Figure 7. Chemical fractionation of (a) EFB and (b) Russian Coal.

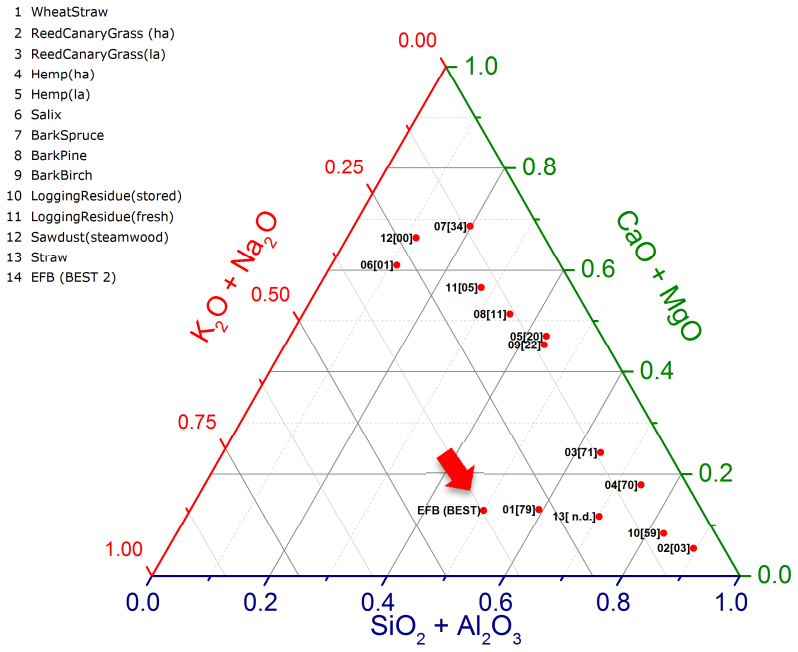

Figure 8: Comparison of composition of EFB with other biomass fuels[14,15]. The number inscribed in [ ] represents the melt fraction reported in the source.

Due to logistic constrains, Russian coal was used to model ASEAN coal. Figure 9 shows the comparison of the Russian coal (model) and Indonesian coal (a type of ASEAN coal).

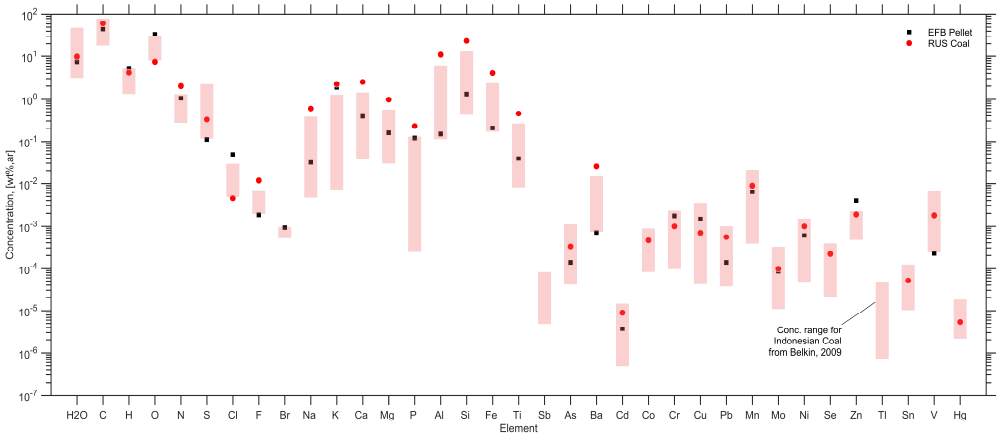

Figure 9: Comparison of EFB, Russian coal (model) and Indonesian coal (a type of ASEAN coal).

3.3 Set of experiments

The test matrix consisted of different fuels blends (Table 3) and measurements (Table 4). Measurement equipment comprised of:

- Basic on-line flue gas analysis by conventional methods (IR: CO_2, CO, SO_2, NO_x paramagnetic: O_2)
- Completing on-line flue gas analysis (HCl, N_2O, NO_2 etc.) by FTIR-spectroscopy
- Deposition probes (superheater simulators) collecting deposits on metal rings kept at metal temperatures simulating most critical positions of superheaters

For Test 1 to 3, limestone was added to control the SO_2 level to 100 ppm (dry, 6% O_2 red.).

Table 3: The test matrix done consisted of a test set with different fuels blends.

Test#	Duration, hr.	Russian bituminous coal, en-%	EFB, en-%	Limestone added
1	11	100%	0%	Ca/S=2.6
2	5	85%	15%	Ca/S=2.0
3	4	74%	26%	Ca/S=1.0
3B	1	74%	26%	no
4	39	66%	34%	no
5	26	56%	44%	no

Table 4: Deposit collections during the test periods.

Test#	Deposition probe before 2nd cyclone		
	500 °C	560 °C	FTIR
1	X	X	
2	X	-	
3	X	-	X
3B	-	-	
4	X	X	
5	X	X	

3.4 Flue gas analysis

The CFB reactor was equipped with a sampling line for on-line analyzer of O_2, CO, CO_2, NO and SO_2 (Servomex 4900). The sample was taken from the flue gas line after gas cooler (see Figure 5). In addition, flue gas sample was taken to a FTIR analyzer through port after primary cyclone through a Hastelloy filter followed by a heated Teflon-coated line which inner surface temperature was maintained at 180 ºC. Concentrations of NO, N_2O, NO_2 and HCl were measured with GASMET^{TM} DX-SERIES analyzer. The accuracy of FTIR was

estimated as 10–15% of the reported concentration value. The detection limit was approximately 1 ppm vol. excluding NO, for which the detection limit was approximately 2 ppm vol.

3.5 Deposit collection and analysis

The fouling rate (mass deposition as g/(m^{2}h)) and deposition of elements have been studied with two deposit probes which are located before and after secondary cyclone (see Figure 5). The surface temperatures of the deposit collection rings can be set with air-cooling to desired values to simulate given superheater tube locations in a selected power plant. The material sleeves of the probes can be removed with the accumulated deposits and cast in resin for further analysis (Figure 10). The standard sleeve material used by VTT is X6 CRNITI 1810. This material is used, if the behavior of some specific material is not studied.

The gas temperature during tests in the sampling point before 2nd cyclone was 808-829 °C. The collection rings were both 16 mm in diameter. The ring length in the probe was 30 mm. The surface temperatures of the rings were set to 500 and 560 °C. The metal temperature on the lee side was 10-20 °C lower than on the wind side due to differences in heat transfer from the flue gas. The deposit sampling time was two hours.

Elemental analysis was conducted with SEM-EDXA by Top Analytica Oy. A bulk analysis was conducted on few square millimeters of the deposit layer. The samples for these analyses were taken from wind side, lee side and approximately 50 degrees from the wind side (Figure 7).

Figure 10: Deposit sampling ring as a part of the deposition simulator before and after test and ring storing before analysis.

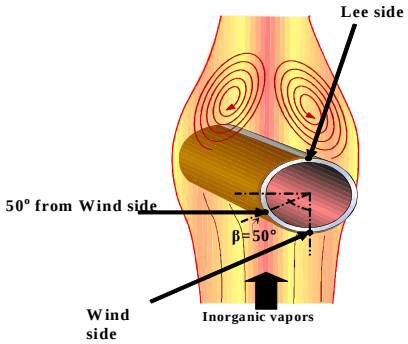

Figure 11: Sampling sites from the deposit probe to SEM-EXDA analysis.

3.6 Reactor conditions

Temperature is presented as function of gas residence time in Figure 12 enabling direct comparison to larger reactors and power plants. The conditions in the 50 kW CFB should simulate well CFB power plant furnaces. The goal was to have ~ 850 °C in the riser. Volatile content in the fuel influences to temperature profile. Temperature increase close to secondary air inlet cannot be avoided (occurring also in power plant furnaces). Shift of the intensive combustion zone upwards in the furnace as function of increased biomass portion can be detected in all sets of experiments. The increase in the share of EFB in fuel blend didn't have great effect on the solid density profiles. Solid density vs. height data (Figure 13) allows comparison to larger reactors and power plants.

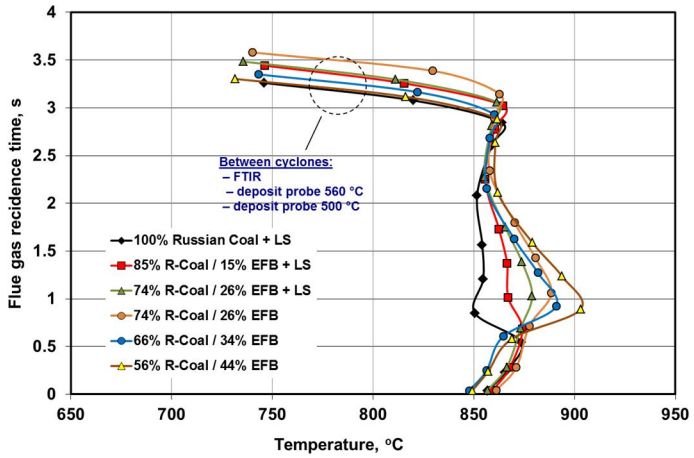

Figure 12: Temperature vs. residence time data during the tests

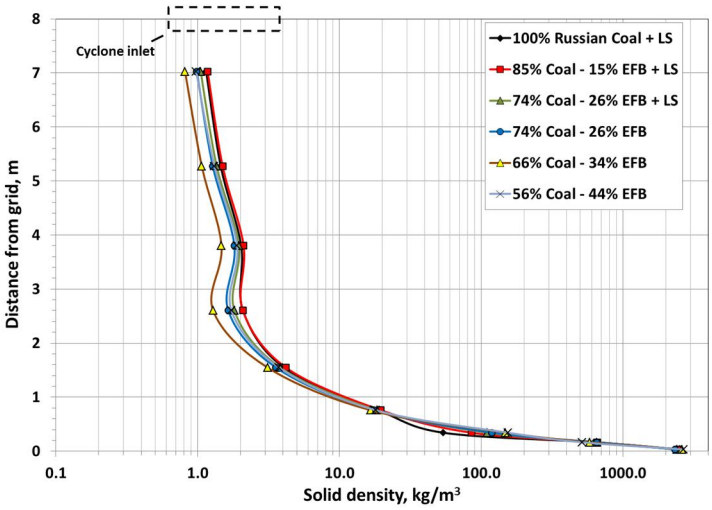

Figure 13: Solid density vs. furnace height during the tests with Russian bituminous coal and straw blends.

4 Results

4.1 Flue gas composition

For all the test, O_2 concentration remained rather well inside the goal value (~ 6% vol.) and concentrations of H_2O, and CO_2 did not vary significantly at different EFB – coal share.

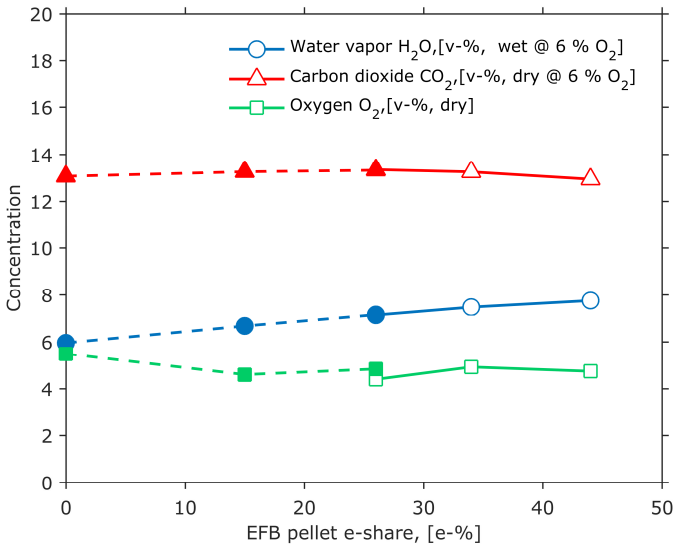

Figure 14: Concentration of the major components (v-% scale) in the flue gas. Filled points represent test points with limestone addition.

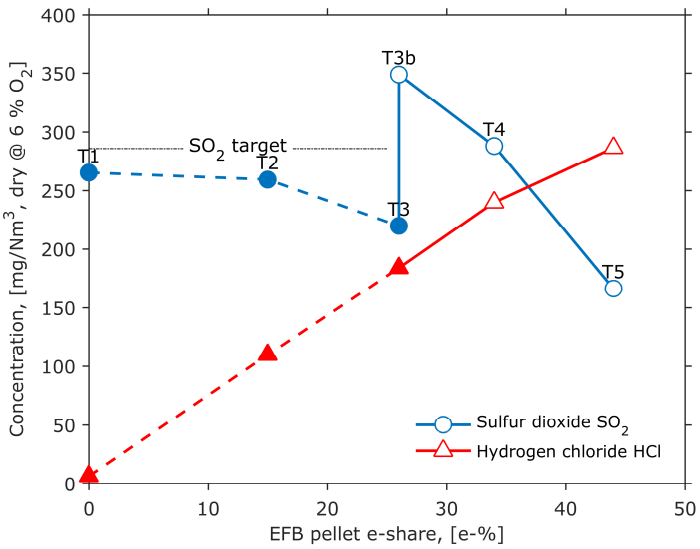

Figure 15: Concentration of the SO_2 and HCl in the flue gas at different EFB share. Filled points represent test points with limestone addition.

SO_2 and HCl concentration are important parameters for emission and corrosion risk monitoring. High SO_2 concentration enables SO_3 formation, which destroys corrosive alkali chlorides (see Eq. 3). Concentration of risky Cl (present in alkali chlorides) can be estimated in a coarse level by subtracting HCl flow from the flow of Cl fed to the furnace (in the fuel). Test 1 - 3 when limestone was added, the SO_2 concentration was keep below the 100-ppm (dry, 6% O_2) target. When limestone addition was halted, the SO_2 concentration increased (see Test 3 and Test 3b in Figure 15). For Test 4 and 5 SO_2 continually decreased even without limestone addition because S in the EFB is just 1/3 that of coal. HCl on the other hand increased monotonously with the EFB share. The concentration of Cl in the EFB is two orders of magnitude higher than that of coal, see Table 3.

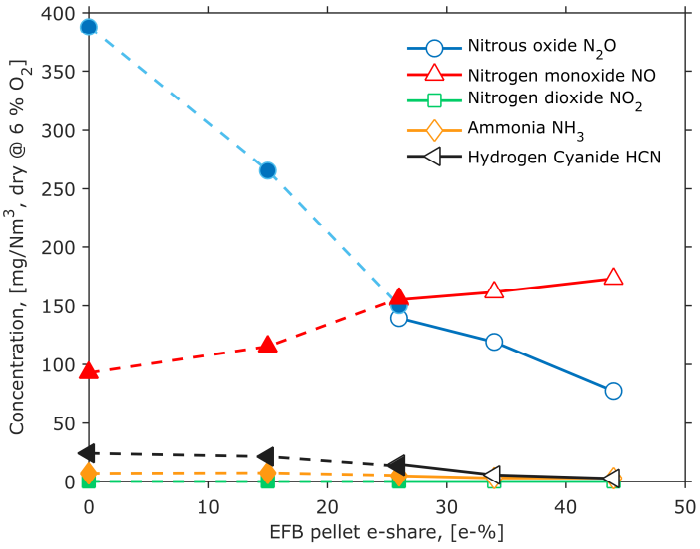

Figure 16: Concentration of nitrogen compounds in the flue gas at different EFB share. Filled points represent test points with limestone addition.

Nitrous oxide (N_2O) and nitrogen monoxide (NO) are the major N-compound measured by the FTIR. A significant reduction of 310 mg N_2O / Nm^3 dry @ 6% O_2 (or ~80% decrease) was measured from Test 1 to 5. NO on the other hand rose by 80 mg / Nm^3 dry @ 6% O_2 (or 87% increase) from Test 1 to 5.

Hämälainen and Aho proposed a theory that if the fuel O/N ratio is high, the conversion of HCN to NH_3 increases because the OH/HCN concentration inside the fuel particle is high [16]. The O/N in the EFB is 28 mol/mol while in the coal it is only 3.3 mol/mol.

The concentration of CO in the flue gas also continuously decreased with increase in EFB share, see Appendix 1.

4.2 Deposition Rate and Deposit Analysis

The complete deposits composition for Test 1 – 5 is in Appendix 2. Si, Al, S, K, and Cl are the dominant elements found in the deposits. This section discusses the deposition rate and deposit composition of these elements at various shares of EFB.

4.2.1 Chlorine

Chlorine has a central role in hot corrosion. Cl deposits as alkali chlorides and attacks the heat transfer surfaces.

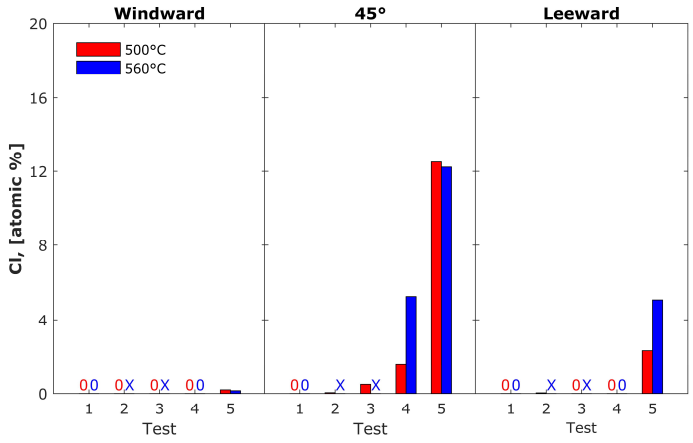

Figure 17: Concentration (in atomic-%) of chlorine collected for probes maintained at 500°C and 560°C metal temperature. 0 = zero atomic-%, X = no data.

The concentration of Cl is negligible in the windward and leeward side in Test 1 to 4, in Test 5 Cl content is < 0.2 atomic-% in the windward side and < 5 atomic-% in the leeward side. In the 45°, Test 1 did not contain Cl, while the rest has minute (0.04 atomic-%, Test 2) to high (12 atomic-%, Test 5) Cl content. In Test 5, the atomic (or molar) ratio of Cl to K is 0.54 (500°C probe) and 0.61 (560°probe), this suggests there is enough K in the deposits that can be present as KCl.

Depending on superheater design, material temperature and grade it is safe to assume the risk of corrosion starts in the rage of 25 en-% to 35 en-% EFB.

4.2.2 Potassium

The potassium in the deposit signals the possible presence of chloride or sulfate ions in the deposit. At the right proportion with Si/Al, K (plus Na[1]) may also result in deposit melting

[1] Na concentration is very low (max < 2 at-%).

In all positions, K concentration tends to increase with EFB en-%. For the 500°C probe, K increased ~8, ~37 and ~8 times in the wind, 45° and lee position, respectively from Test 1 to 5. For the 560°C probe, K increased ~8, ~21 and ~12 times in the wind, 45° and lee position, respectively from Test 1 to 5. In test point 5 and 45° position, K is the most abundant element in the deposit.

The increase in K is clearly linked to the increase share of the K-rich EFB. These results agree with the studies of Madhiyanon et al. [17].

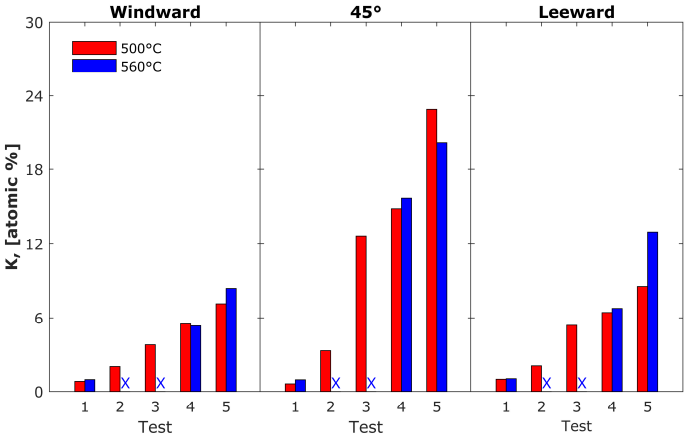

Figure 18: Concentration (in atomic-%) of potassium collected for probes maintained at 500°C and 560°C metal temperature. X = no data.

4.2.3 Sulfur

S can participate in gaseous alkali chloride sulfation and destroy alkali chlorides to form sulfate, or in intra-particle sulfation. The latter is more problematic because it directly produces $Cl_{2(g)}$ inside the deposits [18] via Eqn. 3 and the Deacon oxidation of HCl:

$$2HCl_{(g)} + \frac{1}{2}O_{2(g)} \rightarrow Cl_{2(g)} + H_2O_{(g)} \quad (5)$$

For S, there is a slight increase in concentration at the windward and leeward side as the EFB share is increased. In the 45° position, the increase is more significant from Test 1 to 3; from Test 3 to 5 the concentration has remained constant.

(a)

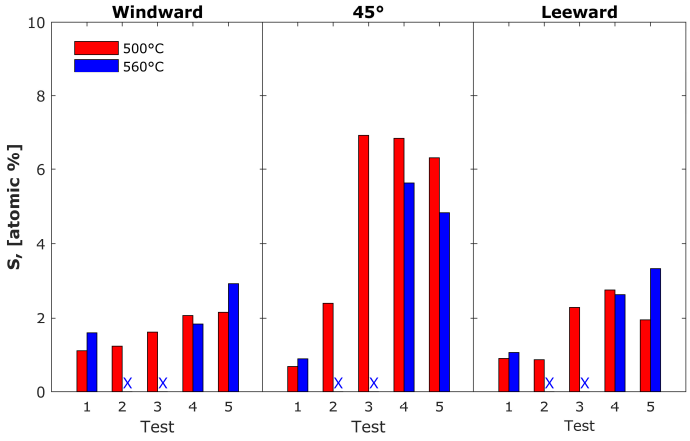

Figure 19: Concentration (in atomic-%) of sulfur collected for probes maintained at 500°C and 560°C metal temperature. 0 = zero atomic-%, X = no data.

4.2.4 Silicon and Aluminum

Deposits that contain mostly Si and Al have low corrosion risks, as these elements do not participate directly in hot-corrosion mechanism.

(a)

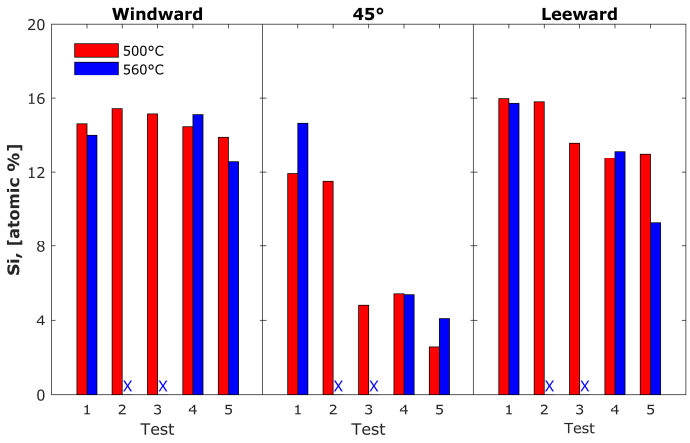

(b)

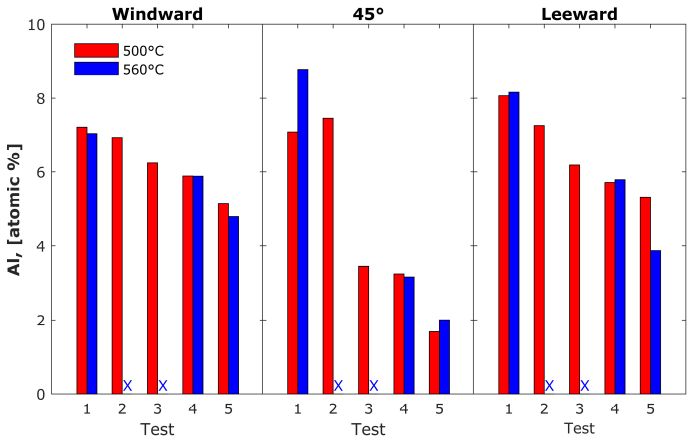

Figure 20: Concentration (in atomic-%) of silicon and aluminum collected for probes maintained at 500°C and 560°C metal temperature. X = no data.

Si dominates the windward and leeward side of the deposit probe and its composition does not vary significantly with EFB share. However, in the 45° position, the composition of Si decreased up to ~1/4 as EFB share is increased from zero en-% to 44 en-%.

In all positions, Al concentration tends to decrease with increased EFB en-%. The biggest decrease is in the 45° position, which is ~ 1/4.

4.2.5 Deposition Rate

Figure 21 shows the calculated deposition rate in the deposit probes simulating the superheaters. Deposition rate is a complex function to several factors e.g. ash flow rate, composition, flue gas conditions etc.

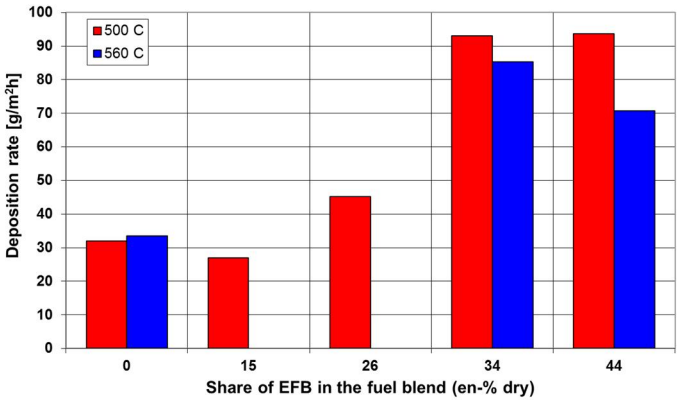

Figure 21: Measured ash deposition rate on the deposit probes.

For Test 1 to 3, the deposition is around 25 – 45 g/m^{2}h, as discussed in the preceding section, the deposits are mainly Si, Al, S, and some K. Si, Al and S may mostly come from the fragmentation of coal. K may come from the EFB.

For Test 4 and 5, a big jump in deposition rate was measured; on average, the deposition rate is 80 g/m^{2}h. This means that the deposition of Cl is high in the probes for these tests, especially for Test 5 where Cl is dominant.

4.3 Formation of KCl – Thermodynamic analysis

To explain the increase in K and Cl in the deposit, formation of KCl was calculated using thermodynamic equilibrium analysis in FactSage. Calculation did not consider limestone addition for Test 1 – 3; it is possible KCl calculated is underestimated. Reactivity factor for coal (calculated from other projects) was incorporated in the calculation. According to the model, the concentration of KCl starts to rise at Test 3, see arrow Figure 22. After Test 3, the concentration of KCl quickly rose. This could partly explain why Cl concentration in the deposit rapidly rose between Test 3 to 5.

The safe share of EFB from alkali chloride induced corrosion point of view depends on superheater design, material temperature and material grade. For mitigating the corrosion risk additives can be injected [12] that will destroy alkali chlorides.

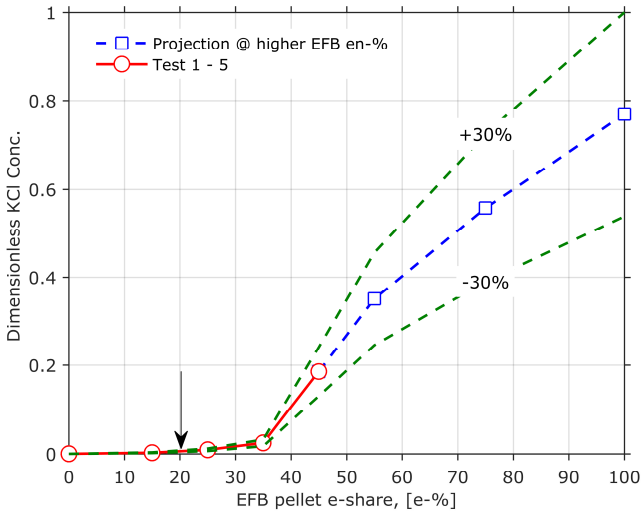

Figure 22: Estimated KCl concentration at air to fuel ratio of 1.35 and T = 700°C to 850°C during combustion of EFB and coal.

4.4 Melting of deposits – Thermodynamic analysis

Deposition is affected by the presence of melt in the deposit layer. When melt is present, the deposits are sticky and deposition is enhanced.

Thermodynamic equilibrium calculation in FactSage is used to model the melting of the deposits. The deposit composition measured in Appendix 2 is assumed uniform in each position (windward, 45°, and leeward). Melting calculations are made at the outermost deposit layer close to the flue gas. We assume that the mass of the flue gas is significantly bigger than the deposits (1000 g flue gas/1 g deposit)

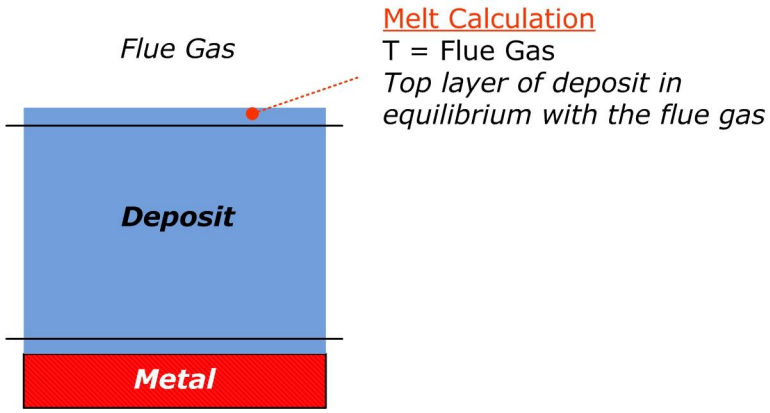

Figure 23: Assumed position and conditions used in the thermodynamic equilibrium calculation.

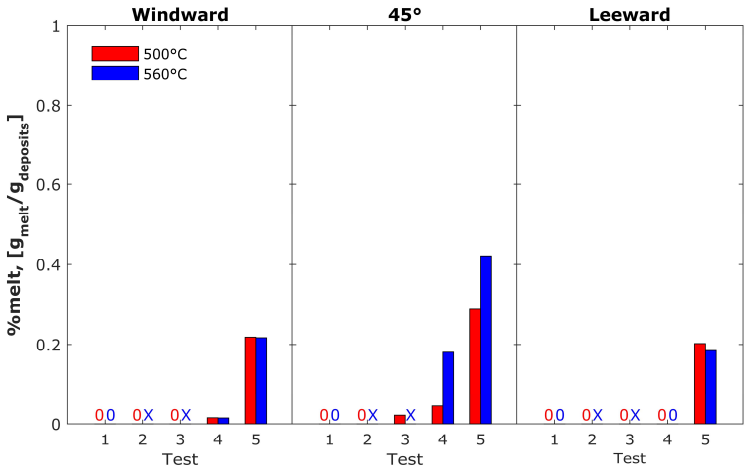

Figure 24: Calculated melt fraction of deposits at different position of the probe.

Formation of melt above the critical 15% happens in the 45° starting from Test 4 (34 en-% EFB), and only in Test 5 (44 en-% EFB) in the windward and leeward position. Formation of both salt and oxide melt was detected. Si, K, Na, Al and S are the major components of the oxide melt; while K, Cl and Na are the major components of the salt melt. In general, at 45° there is more salt melt.

The increase in KCl in the flue gas and melt formation in the deposit, in Tests 4 and 5 explains the increase in the deposition rate measured for these tests.

5 Conclusion and Recommendation

Combustion of EFB up to 44 en-% has been conducted in circulating fluidized bed combustion pilot facility. Emission, fouling, and deposition of critical elements related to combustion of the agro-fuel have been studied. At low EFB share (< 25 en-%) limestone addition might be required to meet the required limit for SO_2 emission. At higher EFB share, SO_2 in the flue gas continuously decreased due to low concentration of sulfur in the EFB.

N_2O concentration, which is typically elevated in coal combustion, continuously decreased and was replaced by NO as the share of the EFB is increased. Minor N-compounds detected are NH_3 and HCN. More tests must be made to ensure that NOx emission is minimized.

Corrosion risk through Cl deposition (by assuming that deposits are corrosive only when Cl is present) was monitored using deposit probes simulating boiler superheaters. In all positions in the probe, K concentration continuously increased as more EFB is burned. Chlorine, the major culprit in corrosion starts to deposit in the probe around 25 en-% to 35 en-% EFB. Finally, at 44 en-% EFB, Cl is the most dominant element in the 45° position of the probe.

Thermodynamic equilibrium analysis reveals that the increase in K and Cl is correlated with the enhanced formation of KCl in the gas phase as more EFB is burned. The increase in KCl in the flue gas and melt formation in the deposit, in Tests 4 and 5 explains the increase in the deposition rate measured for these tests.

Long duration test with higher EFB en-% share must be made to assess applicability of the biofuel in large-scale combustion set-up.

6 References

[1] EEA, 2013, EU bioenergy potential from a resource-efficiency perspective.

[2] EuroStat, 2015, Primary production of renewable energy by type [Online]. Available: http://ec.europa.eu/eurostat/web/products-datasets/-/ten00081.

[3] Bjerg, J., Aden, R., Ogand, J. A., Arrieta, J. A., Hahlbrock, A., Holmquist, L., Kellberg, C., Klp, W. N., Koch, J., Langnickel, U., Nielsen, C., Rising, A., Rizkova, M., Rookmaaker, J., Ryckmans, Y., Ryymin, R., Shier, C., Sochr, D., Tatar, T., and Tolley, A., 2001, Biomass 2020 : Opportunities, Challenges and Solutions, Eurelectric, p. 72.

[4] Aho, M., Envall, T., and Kauppinen, J., 2013, Corrosivity of flue gases during co-firing Chinese biomass with coal at fluidised bed conditions, Fuel Process. Technol., **105**, pp. 82–88.

[5] Becidan, M., Houshfar, E., Khalil, R. A., Skreiberg, Ø., Løv, T., and Sørum, L., 2011, Optimal Mixtures To Reduce the Formation of Corrosive Compounds during Straw Combustion : A Thermodynamic Analysis, Energy & Fuels, **25**, pp. 3223–3234.

[6] Christensen, K. a., Stenholm, M., and Livbjerg, H., 1998, The formation of submicron aerosol particles, HCl and SO2 in straw-fired boilers, J. Aerosol Sci., **29**(4), pp. 421–444.

[7] Silvennoinen, J., and Hedman, M., 2013, Co-firing of agricultural fuels in a full-scale fluidized bed boiler, Fuel Process. Technol., **105**, pp. 11–19.

[8] Bajamundi, C. J. E., Vainikka, P., Hedman, M., Silvennoinen, J., Heinanen, T., Taipale, R., and Konttinen, J., 2015, Searching for a robust strategy for minimizing alkali chlorides in fluidized bed boilers during burning of high SRF-energy-share fuel, Fuel, **155**, pp. 25–36.

[9] Wolf, K. J., Mu, M., Hilpert, K., and Singheiser, L., 2004, Alkali Sorption in Second-Generation Pressurized Fluidized-Bed Combustion, Energy & Fuels, **18**, pp. 1841–1850.

[10] Backman, R., Khalil, R. a., Todorovic, D., Skreiberg, Ø., Becidan, M., Goile, F., Skreiberg, A., and Sørum, L., 2013, The effect of peat ash addition to demolition wood on the formation of alkali, lead and zinc compounds at staged combustion conditions, Fuel Process. Technol., **105**, pp. 20–27.

[11] Aho, M., and Ferrer, E., 2005, Importance of coal ash composition in protecting the boiler against chlorine deposition during combustion of chlorine-rich biomass, Fuel, **84**(2-3), pp. 201–212.

[12] Aho, M., Vainikka, P., Taipale, R., and Yrjas, P., 2008, Effective new chemicals to prevent corrosion due to chlorine in power plant superheaters, Fuel, **87**(6), pp. 647–654.

[13] Lahijani, P., and Zainal, Z. A., 2011, Gasification of palm empty fruit bunch in a bubbling fluidized bed: A performance and agglomeration study, Bioresour. Technol., **102**(2), pp. 2068–2076.

[14] Lindstro, E., Gilbe, C., Marcus, O., Bostro, D., Backman, R., Samuelsson, R., and Burvall, J., 2008, Slagging Characteristics during Residential Combustion of Biomass Pellets, (5), pp. 3536–3543.

[15] Gilbe, C., Lindstro, E., Backman, R., Samuelsson, R., Burvall, J., and Marcus, O., 2008, Predicting Slagging Tendencies for Biomass Pellets Fired in Residential Appliances : A Comparison of Different Prediction Methods, (7), pp. 3680–3686.

[16] Hämäläinen, J. P., and Aho, M. J., 1996, Conversion of fuel nitrogen through HCN and NH3 to nitrogen oxides at elevated pressure, Fuel, **75**(12), pp. 1377–1386.

[17] Konsomboon, S., Pipatmanomai, S., Madhiyanon, T., and Tia, S., 2011, Effect of kaolin addition on ash characteristics of palm empty fruit bunch (EFB) upon combustion, Appl. Energy, **88**(1), pp. 298–305.

[18] Grabke, H. J., Reese, E., and Spiegel, M., 1995, The Effects of Chloride, Hydrogen Chloride and Sulfur Dioxide in the Oxidataion of Steels Below Deposits, Corros. Sci., **37**(7), pp. 1023–1043.

Appendix 1: CO concentration at different EFB shares

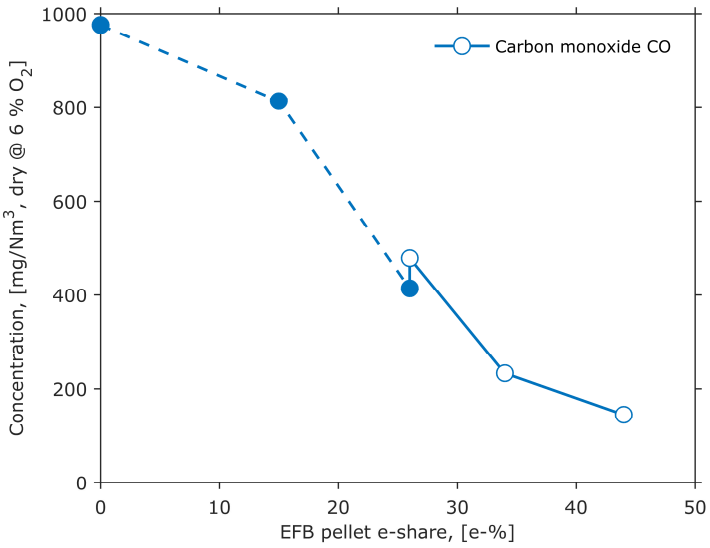

Appendix 2: Deposit Composition

Metal temp. = 500°C

Metal temp. = 560°C